Journal of Power Sources 196 (2011) 5122–5127

Contents lists available at ScienceDirect

Journal of Power Sources

journal homepage: www.elsevier.com/locate/jpowsour

Short communication

Nickel–tin foam with nanostructured walls for rechargeable lithium battery

Hye-Ran Jung[a], Eun-Ji Kim[a], Yong Joon Park[b], Heon-Cheol Shin[a,*]

[a] School of Materials Science and Engineering, Pusan National University, San30, Jangjeon-dong, Keumjung-ku, Busan 609-735, Republic of Korea
[b] Nuclear Chemistry Research Division, Korea Atomic Energy Research Institute, Dukjin-dong 150-1, Yuseong-gu, Daejeon 305-353, Republic of Korea

ARTICLE INFO

Article history:
Received 13 December 2010
Received in revised form 24 January 2011
Accepted 30 January 2011
Available online 17 February 2011

Keywords:
Nickel–tin alloy
Foam
Nanostructure
Electrochemical deposition
Lithium battery

ABSTRACT

Nickel–tin foams with a graded micro-porous framework and nano-porous walls are created by an electrochemical deposition method for use as the anode in rechargeable lithium batteries. The resulting electrodes react readily with lithium electrochemically and deliver a reversible capacity of more than 470 mAh g^{-1} for up to 50 cycles. In addition, they show outstanding rate performance: their reversible capacity at a discharging rate of 20 C is about 70% of the capacity at a rate of 1 C, due mainly to their unique structure which allows facile lithium-ion transport and fast surface reactions. The reversible capacity and rate capability show strong dependence on the thickness of the deposit and this is associated with the accessibility of lithium ions inside the porous structure.

1. Introduction

There has been strong demand for advanced lithium batteries to meet the energy requirements for portable electronic devices with multi-functionality and for eco-friendly transportation systems. With regard to the electrode materials, recent effort has been focused mainly on tin- and silicon-based anodes together with high-voltage cathodes [1–3]. In spite of the fact that the theoretical capacity of tin is lower than that of silicon, the comparative ease with which various structures and alloy types can be prepared from tin has attracted the attention of researchers. Basically, tin undergoes a large reaction-induced volume change that results in internal mechanical strain. In particular, the tensile strain during the delithiation (or dealloying) process severely affects its structural integrity and results in deterioration of the cycleability.

Among the various useful tin-based compounds that have been developed, those include an inactive element (*e.g.*, nickel, cobalt, copper, and iron) have been considered as promising material types [4–9]. Their reaction with lithium is described as producing brittle lithium–tin active phases within a ductile inactive matrix that buffers the large volume change of the active phases, leading to improved cycleability. Although, in general, cycling stability and specific capacity are mutually exclusive, tin-based compounds still have good potential for use as next-generation anode materials. In a further attempt to enhance their performance, nano-porous structures were prepared with the intention of accommodating the volume change and also providing a large reaction area. Some of the studies in this area reported notable cycling performances [10,11].

In this regard, pore gradient copper–tin (η'-Cu_6Sn_5) foam with a micro-porous framework and nano-porous walls was recently created by an electrochemical deposition process [12]. In addition to the buffering effect of the inactive copper matrix, its porous structure provides the space required for free volume expansion, which might effectively suppress the mechanical disintegration of the electrode during the operation of the cell. Furthermore, since its micro-framework facilitates the rapid transport of lithium ions inside the structure and the nano-porous walls assure a fast interfacial redox reaction, this structure is expected to have the inherently low concentration and activation polarization that are essential for achieving high-rate capability. The resultant porous copper–tin alloy showed superior rate performance, as expected. There were a number of cracks, however, even in the as-prepared sample and this indicates that it had poor mechanical properties, and some aspects of the battery performance (*e.g.*, the cycleability, initial irreversible capacity, and charge–discharge efficiency) were unacceptable.

In this communication, pore gradient nickel–tin micro-foam with nano-structured walls is prepared for use as the anode in rechargeable lithium batteries. The morphology and composition of the as-prepared sample are examined at different deposition times. Its electrochemical properties are investigated by conducting a galvanostatic charge–discharge experiment. In particular, the change in the micro- and nano-porous structure is analyzed in the course

* Corresponding author. Tel.: +82 51 510 3099; fax: +82 51 512 0528.
E-mail address: hcshin@pusan.ac.kr (H.-C. Shin).

0378-7753/$ – see front matter © 2011 Elsevier B.V. All rights reserved.
doi:10.1016/j.jpowsour.2011.01.110

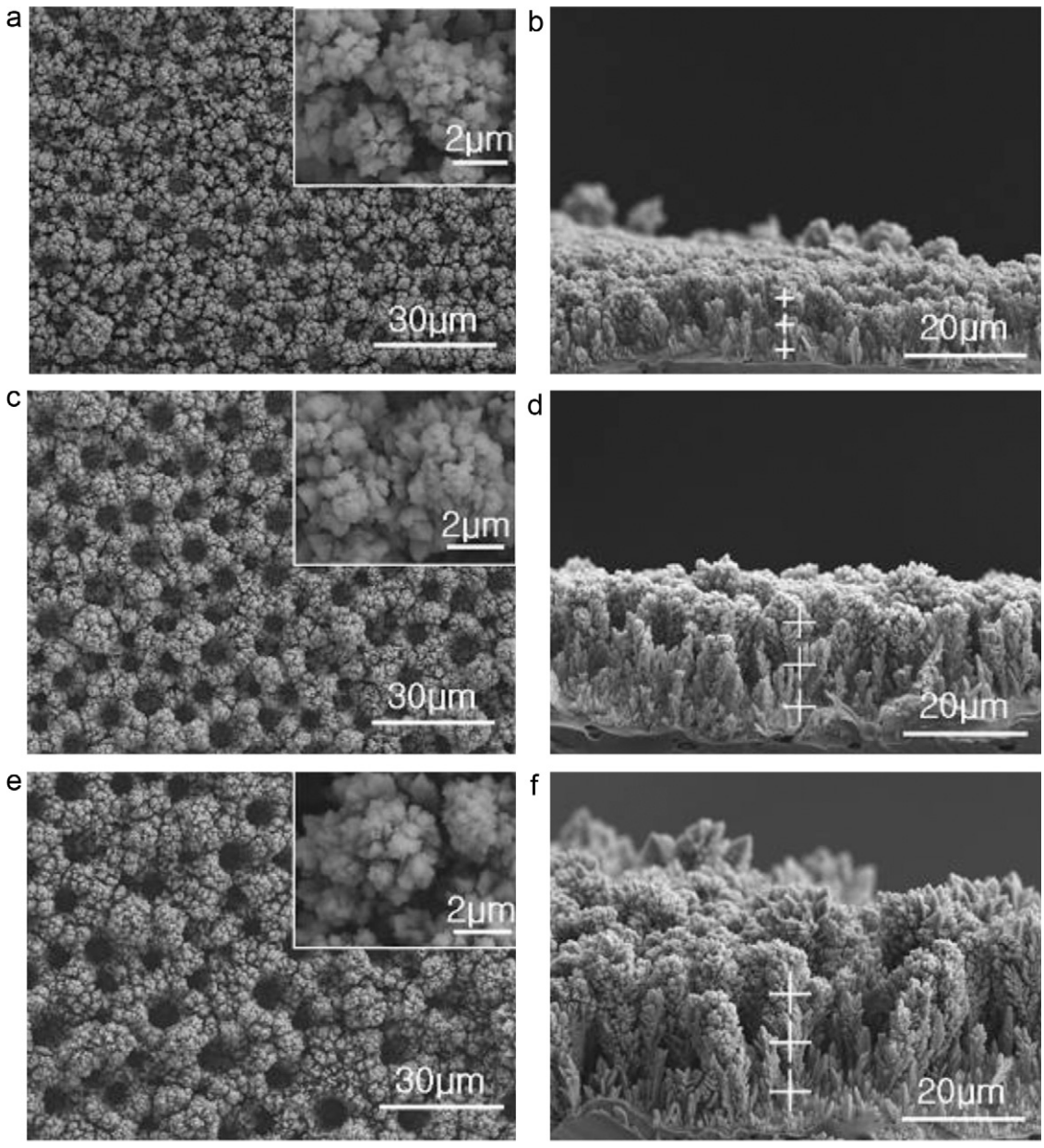

Fig. 1. Top (left) and cross-sectional (right) views of nanostructured nickel–tin foams, created at different deposition times: (a)–(b) 10 s, (c)–(d) 20 s, (e)–(f) 30 s.

of repetitive cycling. Furthermore, its rate capability is evaluated to demonstrate its feasibility for high-power applications.

2. Experimental details

For the preparation of the porous nickel–tin electrodeposits, a copper foil (Alfa Aesar, 99.8%), pre-treated in diluted sulfuric acid to remove the native surface oxide, was used as the working electrode (the cathode) and platinum wire was adopted for the counter electrode (the anode). The distance between the anode and cathode was kept at 1 cm. A constant cathodic current of 2 A cm^{-2} was applied for 10, 20 and 30 s to obtain nickel–tin electrodeposits using an EG&G 263A potentiostat/galvanostat. The plating bath contained 0.075 M $NiCl_2$, 0.175 M $SnCl_2$, 0.15 M NH_2CH_2COOH (glycine), 0.4 M $K_4P_2O_7$, 5 ml l^{-1} NH_4OH, and 1 M H_3PO_4. Glycine and $K_4P_2O_7$ played the role of complexing agents to reduce the difference in the reduction rates between the nickel and tin ions [13–15], while phosphoric acid was selected to generate hydrogen bubbles (a dynamic template for building the foams) during the plating, instead of the sulfuric acid that is usually used [12,16,17], because the latter causes an undesirable side-reaction with $K_4P_2O_7$, leading to the precipitation of K_2SO_4.

The morphologies and chemical compositions of the samples were examined with a scanning electron microscope (Field-Emission SEM, S-4800, Hitachi, Japan) and an energy-dispersive X-ray spectrometer (EMAX, 7593-H, Horiba, Japan), respectively. For structural characterization, powders scratched from the substrate were analyzed by X-ray diffraction (X-Ray Diffractometer, D8 Advance, Bruker, Germany).

For the electrochemical tests, porous nickel–tin electrodeposits on the copper substrate and lithium foil were used as the working and counter electrodes, respectively. The electrolyte was a 1 M solution of lithium hexafluorophosphate ($LiPF_6$) in a 1:1 volume mixture of ethylene carbonate (EC) and diethyl carbonate (DEC). A two-electrode stainless-steel cell (Hohsen Corp., Japan) was adopted for all of the electrochemical measure-

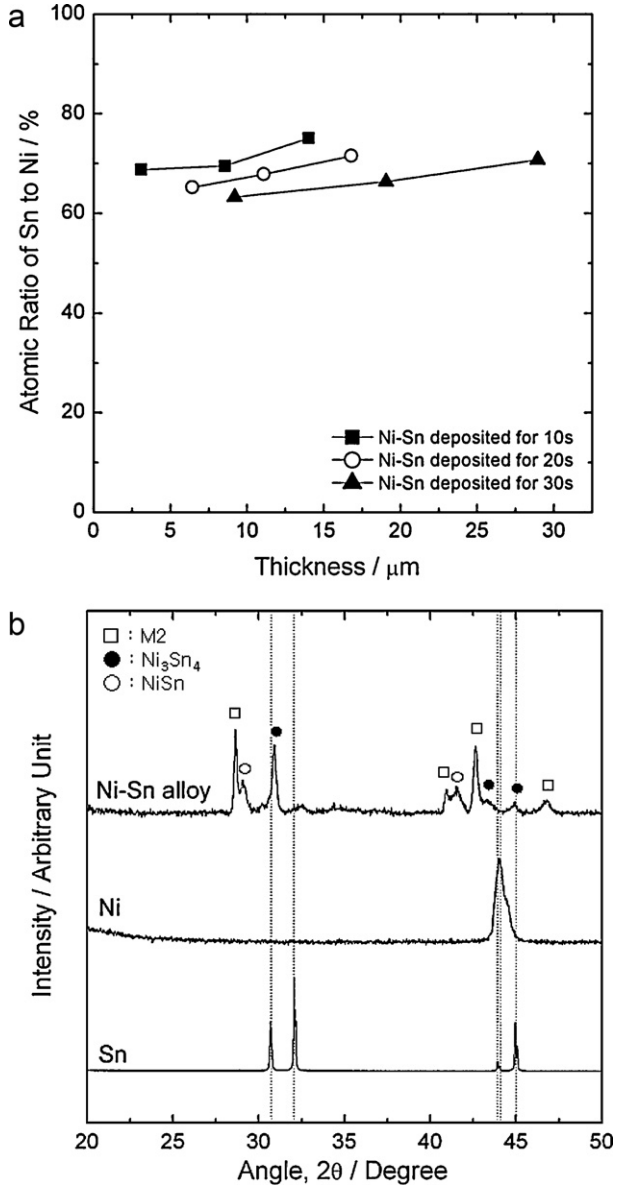

Fig. 2. (a) Atomic ratio of tin to nickel inside deposits. Local composition analyzed for lower, middle and upper parts of cross-sections, as indicated in Fig. 1(b), (d), and (f), respectively, and (b) X-ray diffraction patterns of nickel–tin powders scratched from substrate. Diffraction patterns of pure tin and nickel are given for sake of comparison.

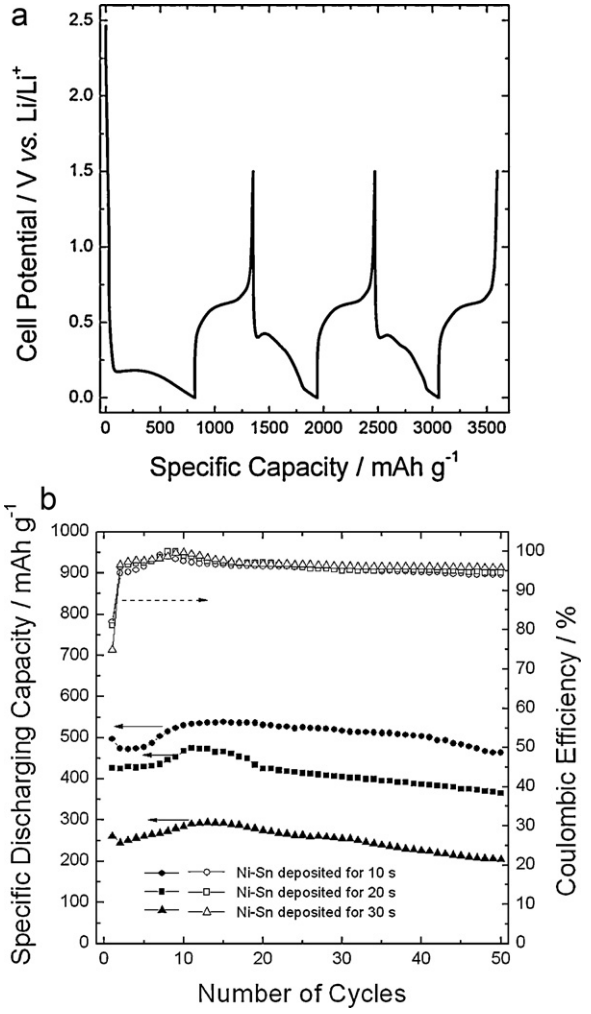

Fig. 3. (a) Typical voltage profiles of sample created for 10 s for first three cycles at 1 C, and (b) dependence of discharging (lithium dealloying) capacity retention and coulombic efficiency on number of cycles obtained for samples created at different deposition times.

ments. In particular, a Teflon O-ring with a thickness of 500 μm was inserted between the nickel–tin electrode and lithium foil, and the former electrode was placed inside the O-ring to prevent any mechanical damage to the porous structure during cell assembly.

Cycleability was evaluated at constant current densities of 0.67, 1.54 and 3.08 mA cm^{-2} for nickel–tin electrodes deposited for 10, 20 and 30 s, respectively, which correspond to 1 C rate for all of the samples. For rate capability tests, the samples were (cathodically) charged at 1 C until the cell potential reached 0 V *vs.* Li/Li$^+$ and subsequently (anodically) discharged at rates ranging from 1 C and 40 C until the cell potential reached 1.5 V *vs.* Li/Li$^+$. A Solartron 1287 potentiostat was employed to perform the galvanostatic cell cycling. All of the cells were assembled and tested in a glove box (MBraun, Germany) filled with purified argon gas.

3. Results and discussion

The top and cross-sectional views of nickel–tin foams created at different deposition times are presented in Fig. 1. The size of the surface pores increases with increasing deposition time and the foam walls become thicker, which is consistent with previous reports [12]. It is noted that the overall foam structure is well constructed with no evidence of the wall cracking that is usually observed in copper–tin alloys with a similar structure. The absence of cracks indicates that the strength of the nickel–tin foam walls is sufficiently high to resist the mechanical stress induced by the great quantity of hydrogen bubbles generated under severe deposition conditions, unlike in the case of copper–tin foam walls.

A closer look at the foam wall reveals that particles with an irregular shape and a size of hundreds of nanometers are combined to form nanoporous spherical aggregates with a diameter of less than several micrometers (insets in Fig. 1). Also, numerous aggregates became loosely connected to each other, leaving additional free space between them. A highly porous structure is uniformly created throughout the deposits, as demonstrated in their cross-sectional views. The unique porous structure of the nickel–tin deposits is well suited for high-power applications where rapid transport of lithium ions to the electrode|electrolyte interface and subsequent fast interfacial reaction are required.

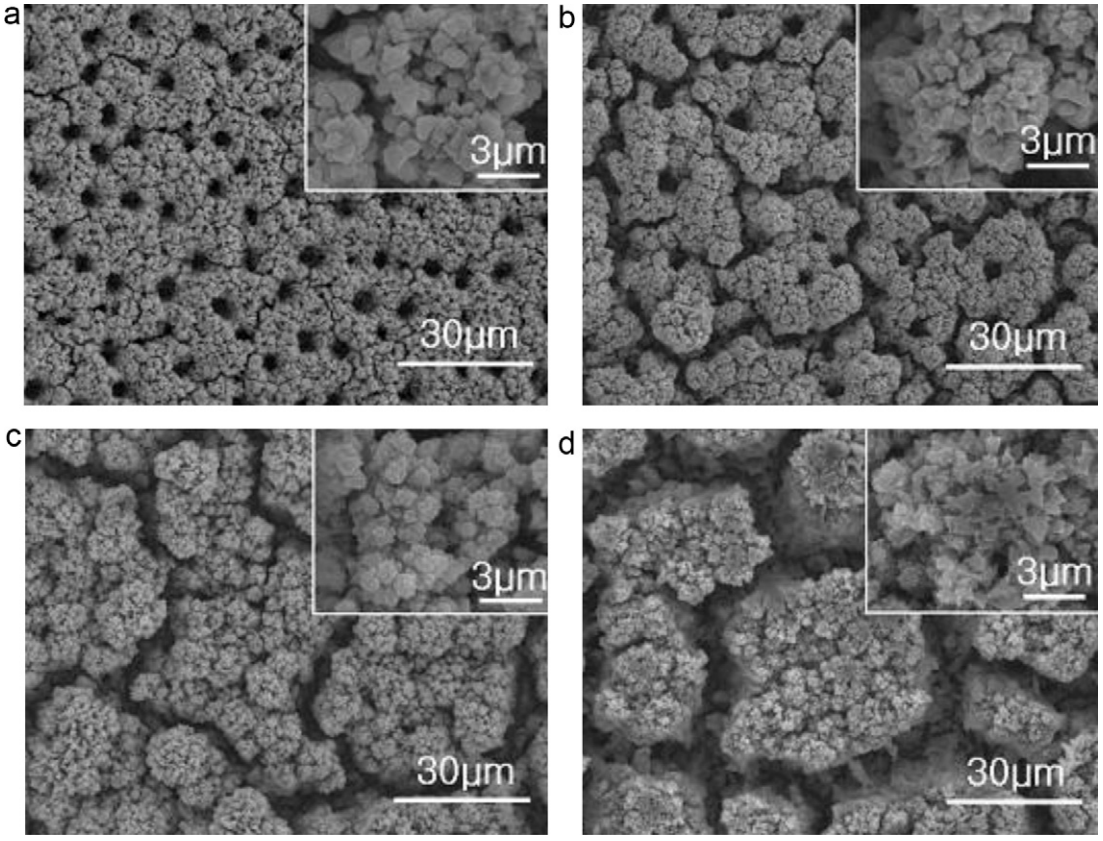

Fig. 4. Change in surface morphology of sample created for 20 s with charge–discharge cycling. (a) After first charging (lithium alloying) process; (b) after subsequent first discharging (lithium dealloying) process; (c) after 30th cycle; (d) after 50th cycle.

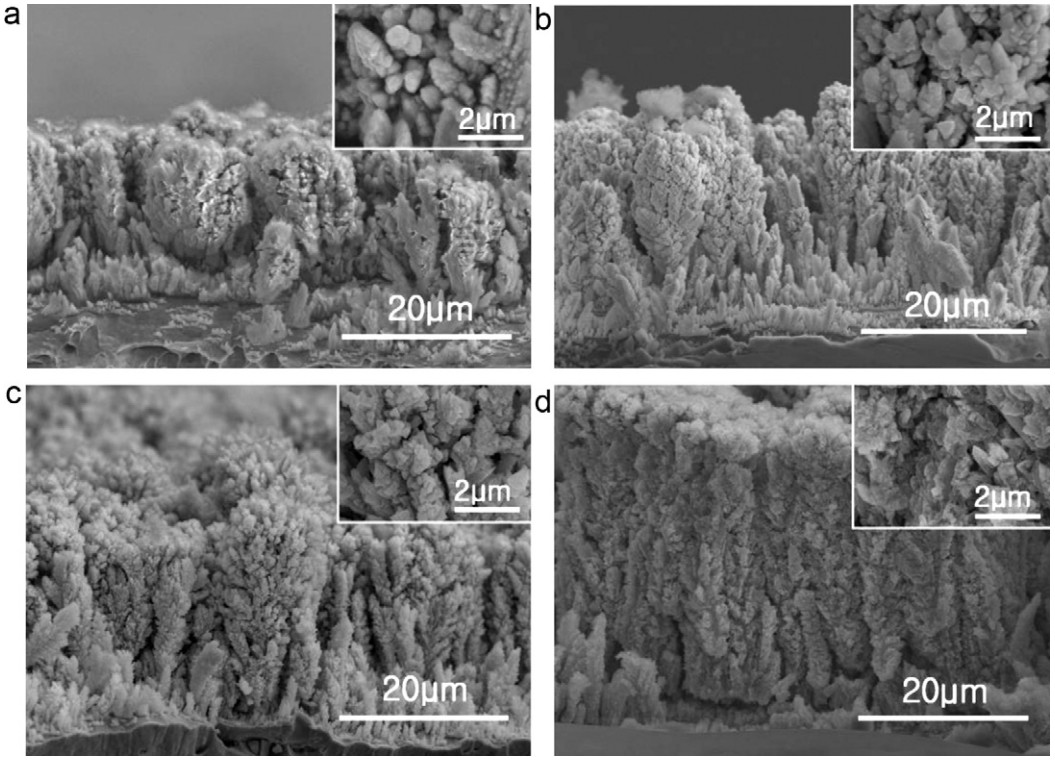

Fig. 5. Cross-sectional views corresponding to Fig. 4(a)–(d).

The atomic proportion of tin in the deposits ranges from 60 to 80%, as shown in Fig. 2(a). The tin content appears to increase slightly with increasing distance away from the substrate and the thicker deposits show a lower average tin content, although the reasons for this have yet to be determined. The XRD patterns of powder scratched from the substrate reveal that the electrodeposits consist of Ni_3Sn_4, NiSn, and an Sn-rich metastable phase (Fig. 2(b)) [4,18]. The presence of the Sn-rich phase explains why the atomic fraction of tin in the deposits exceeds 57%, which is the expected atomic fraction of tin in Ni_3Sn_4.

A typical voltage profile for the porous nickel–tin electrodeposit for the first three cycles is given in Fig. 3(a). The deposit is well lithiated and delithiated as an anode in a rechargeable lithium battery. Moreover, it retains about 85% of its maximum reversible capacity after 50 cycles with high coulombic efficiency, as presented in Fig. 3(b), and this corresponds to a much higher cycleability than that of the porous copper–tin alloys previously reported [12]. In particular, the sample deposited for 10 s delivered a reversible capacity of more than 470 mAh g^{-1} for up to 50 cycles. It is noted that the specific reversible capacity decreases significantly with increasing thickness of the sample. This strongly indicates that it becomes more difficult for the electrolyte (or the lithium ions within it) to reach deep inside the porous structure as the foam wall becomes thicker, leading to a large amount of electrochemically inactive surface or volume. In this respect, it is further noteworthy that the capacity gradually increases for the first 10–15 cycles, as shown in Fig. 3(b). The most plausible reason for this is a cycling-induced opening of the inactive surface due to the repetitive volume expansion and contraction.

The above explanation of the abnormal capacity rise is supported by the morphological change of the deposit in the course of charge–discharge cycling, as presented in Fig. 4. The volume expansion after the first charging process results in a much smaller pore size in both the foam framework and foam walls, as well as increasing particle size (Fig. 4(a)), as compared with those of the as-prepared sample (Fig. 1(c)). Nevertheless, the internal compressive stress arising from lithium alloying does not mechanically destroy the structure of the deposits. By contrast, the structural integrity of the deposits is deleteriously affected during subsequent discharging. That is, the lithium-dealloying-induced tensile stress leads to the formation of numerous cracks in the deposits and causes the foam to lose its structural continuity (Fig. 4(b)). The destruction of the foam walls causes their normally inactive interior surface to be exposed to the electrolyte and, hence, to become involved in the electrode reaction, and this may be the reason for the rise in the specific capacity.

It is interesting to note that the number of micro-sized pores in the foam structure abruptly decreases after the first cycle. It appears that the pores, especially those with a relatively small size, disappear during cyclic expansion and contraction of the neighbouring particles, while the other pores with a large size become part of the cracks in the deposits. Since the thin walls surrounding the large pores are comparatively vulnerable to tensile stress, as compared with the thick walls near the small pores, they are readily broken, causing the pairs of adjacent pores to become connected to each other to produce cracks. When such small cracks come together, they may converge into a continuous long crack.

After several tens of cycles, the micro-sized pores are no longer observed and the deposit loses its foam structure (Fig. 4(c)). Instead, it is characterized by porous islands with a diameter of several tens of micrometers. In spite of the destruction of the foam structure, the resulting structure may still ensure the facile access of the lithium ions to the internal porous structure of the islands, owing to adjacent cracks. The island structure does not change on further cycling in terms of the overall shape and size of the islands, except for a widening of the cracks (Fig. 4(d)). Moreover, the nanostructures

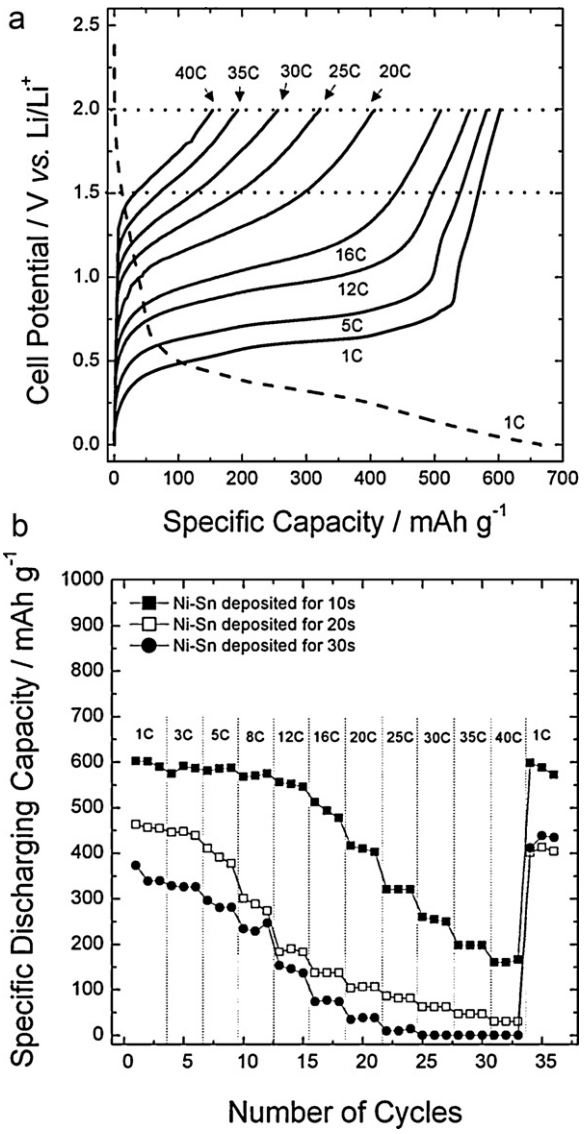

Fig. 6. (a) Typical voltage profiles of sample created for 10 s at different discharging rates; (b) variation of capacity retention with discharging rate obtained for samples created at different deposition times.

inside the islands retain their initial character, with little structural modification of the particles (insets of Fig. 4). This behaviour with cycles is essentially the same throughout the deposits, as presented in Fig. 5.

The reason for the structural modification of the particles has yet to be determined. Nevertheless, the development of a thick solid electrolyte interface layer on the surface, together with the stress-induced structural transformation, may be responsible for the morphological change of the particles [19]. Further investigation is needed to clarify the origin of this process.

The typical voltage profiles obtained for a porous nickel–tin alloy deposited for 10 s at different discharging rates and a summary of the rate performance, is given in Fig. 6(a) and (b), respectively. At discharging rates of 20 C and 30 C, the sample created for 10 s retains about 70 and 40% of the capacity observed at a rate of 1 C when the upper cut-off voltage was 2.0 V *vs.* Li/Li^+. Even when the cut-off voltage is lowered to 1.5 V *vs.* Li/Li^+, respective high capacity retentions of 50 and 20% are observed. This is outstanding rate performance and exceeds that of the tin-based alloys reported previously, that include copper–tin alloys with a structure similar to that of the sample prepared in this work. Although the capac-

ity retention decreases with increasing thickness of the deposit (Fig. 6(b)), the samples deposited for 20 s and 30 s still display excellent rate capabilities.

4. Conclusions

Nickel–tin electrodeposits with a graded microporous framework and nanoporous walls have been created and their electrochemical properties have been evaluated for use as the anode in rechargeable lithium batteries. The reversible capacity of a sample prepared for 10 s remains above 470 mAh g^{-1} for up to 50 cycles, but the capacity falls with increasing thickness, due primarily to the difficulty for the lithium ions to penetrate into the thick walls. During the course of cycling, the overall structure transforms from a foam- to an island-type with little modification of its internal nanostructure. The reversible capacity at a discharging rate of 20 C is about 70% of the capacity at a rate of 1 C and exhibits a dependence on the thickness. This exceptional rate capability is ascribed to the fast transport of lithium ions into the highly open porous structure, the large surface area available for the electrochemical reaction, and the short length for solid-state lithium diffusion through the nanoparticles.

Acknowledgements

The research was supported by the Basic Science Research Program through the National Research Foundation of Korea (NRF) funded by the Ministry of Education, Science and Technology (KRF-2006-331-D00713). Furthermore, the work was partially supported by the Converging Research Center Program (2010K001091) and the NCRC (National Core Research Center) program through the National Research Foundation of Korea funded by the Ministry of Education, Science and Technology (2010-0001-226).

References

[1] I.A. Courtney, J.R. Dahn, J. Electrochem. Soc. 144 (1997) 2045.
[2] M. Wachtler, M. Winter, J.O. Besenhard, J. Power Sources 105 (2002) 151.
[3] B.A. Boukamp, G.C. Lesh, R.A. Huggins, J. Electrochem. Soc. 128 (1981) 725.
[4] T. Watanabe, T. Hirose, K. Arai, M. Chikazawa, J. Japan Inst. Metals 63 (1999) 496.
[5] H. Mukaibo, T. Sumi, T. Yokoshima, T. Momma, T. Osaka, Electrochem. Solid-State Lett. 6 (2003) A218.
[6] N. Tamura, A. Fujimoto, M. Kamino, S. Fujitani, Electrochim. Acta 49 (2004) 1949.
[7] S.D. Beattie, J.R. Dahn, J. Electrochem. Soc. 150 (2003) A894.
[8] W. Choi, J.Y. Lee, H.S. Lim, Electrochem. Commun. 6 (2004) 816.
[9] O. Mao, J.R. Dahn, J. Electrochem. Soc. 146 (1999) 414.
[10] K. Nishikawa, K. Dokko, K. Kinoshita, S.W. Woo, K. Kanamura, J. Power Sources 189 (2009) 726.
[11] L. Huang, H.B. Wei, F.S. Ke, X.Y. Fan, J.T. Li, S.G. Sun, Electrochim. Acta 54 (2009) 2693.
[12] H.-C. Shin, M. Liu, Adv. Funct. Mater. 15 (2005) 582.
[13] V.V. Orekhova, I.D. Roi, Soviet Electrochem. 27 (1991) 638.
[14] M. Ishikawa, H. Enomoto, M. Matsuoka, C. Iwakura, Electrochim. Acta 40 (1995) 1663.
[15] I. Mizushima, M. Chikazawa, T. Watanabe, J. Electrochem. Soc. 143 (1996) 1978.
[16] H.-C. Shin, J. Dong, M. Liu, Adv. Mater. 15 (2003) 1610.
[17] H.-C. Shin, M. Liu, Chem. Mater. 16 (2004) 5460.
[18] M.K. Bhargava, K. Schubert, J. Less-Common Met. 33 (1973) 181.
[19] D.-T. Shieh, J. Yin, K. Yamamoto, M. Wada, S. Tanase, T. Sakaia, J. Electrochem. Soc. 153 (2006) A106.